Spectroscopic signatures of ozone at the air–water interface and photochemistry implications

Josep M. Anglada[a,1], Marilia Martins-Costa[b,c,1], Manuel F. Ruiz-López[b,c,1], and Joseph S. Francisco[d,1]

[a]Departament de Química Biològica i Modelització Molecular (Institut de Química Avançada de Catalunya–Consejo Superior de Investigaciones Cientificas), E-08034 Barcelona, Spain; [b]Laboratoire Structure et Réactivité des Systèmes Moléculaires Complexes, University of Lorraine, 54506 Vandoeuvre-lès-Nancy, France; [c]Centre National de la Recherche Scientifique (Joint Research Unit 7565), 54506 Vandoeuvre-lès-Nancy, France; and [d]Department of Chemistry, Purdue University, West Lafayette, IN 47907-2084

Contributed by Joseph S. Francisco, June 27, 2014 (sent for review June 8, 2014)

First-principles simulations suggest that additional OH formation in the troposphere can result from ozone interactions with the surface of cloud droplets. Ozone exhibits an affinity for the air–water interface, which modifies its UV and visible light spectroscopic signatures and photolytic rate constant in the troposphere. Ozone cross sections on the red side of the Hartley band (290- to 350-nm region) and in the Chappuis band (450–700 nm) are increased due to electronic ozone–water interactions. This effect, combined with the potential contribution of the $O_3 + h\nu \rightarrow O(^3P) + O_2(X^3\Sigma_g^-)$ photolytic channel at the interface, leads to an enhancement of the OH radical formation rate by four orders of magnitude. This finding suggests that clouds can influence the overall oxidizing capacity of the troposphere on a global scale by stimulating the production of OH radicals through ozone photolysis by UV and visible light at the air–water interface.

atmospheric chemistry | heterogeneous processes | reactive oxidant species | computer simulations

Ozone, which is generated in the stratosphere, is well known to strongly absorb solar radiation in the UV region and contribute to the radiative forcing of the atmosphere, thereby influencing climate (1, 2). Changes in ozone abundances can perturb UV radiation levels in the atmosphere and at Earth's surface, and thus the extensive quantification of ozone distributions is critical to understanding its impact on the global environment. Stratospheric ozone distribution changes can affect the temperature in the stratosphere as well as impact photochemical processes in the troposphere. Tropospheric ozone can be produced photochemically in situ or transported down from the stratosphere. Tropospheric ozone exhibits significant radiative forcing, because O_3 is a greenhouse gas, but it also acts as a pollutant; its concentration is one of the measures to indicate the air quality worldwide.

The photochemistry of ozone in the troposphere is, on the other hand, an important source of hydroxyl radicals, which are key to the chemistry of the atmosphere and determine the fate of anthropogenically emitted organic compounds (3). Hydroxyl radicals are mainly produced through the reactions

$$O_3 + h\nu(\lambda < 310\ \text{nm}) \rightarrow O(^1D) + O_2 \quad [1]$$

$$O(^1D) + H_2O \rightarrow 2OH, \quad [2]$$

although a fraction of the formed $O(^1D)$ atoms can also react with methane according to

$$O(^1D) + CH_4 \rightarrow OH + CH_3. \quad [3]$$

Field measurements over the equatorial Pacific found significant variability of tropospheric ozone and hydroxyl radical concentrations, which has been suggested to affect the oxidizing efficiency of the troposphere (4). On the other hand, different experiments have suggested that current atmospheric models are missing a source of OH radicals. Discrepancies between models and observations in forested and polluted environments, for instance, indicated that OH chemistry is not fully understood (5–8). Frost and Vaida (9) were the first to propose that ozone in the low atmosphere could form a weakly bound complex with water, whose photodissociation could account for up to 15% of the available OH in the troposphere. The implicit assumption is that the long-wavelength absorption of ozone may be enhanced as a result of complexation with water, i.e., $\lambda > 411$ nm. Shifts in the O_3 spectrum as a function of the environment have been reported in the literature (10, 11). This makes the absorption of UV/visible radiation by O_3-H_2O an important factor in the accurate quantification of the complex's photochemical contribution to OH abundances. Experiments by Hurwitz and Naaman (12) show that photodissociation through irradiation with 355 nm generated a quantum yield of the hydroxyl radical of 1%. However, experiments by Jin et al. (13) observed no UV absorption by the complex at 351.8 nm and hence found the contribution of OH from UV photolysis of the complex to be an insignificant source of OH at this wavelength. Axson et al. (14) carried out cavity ring down measurements in the Huggins–Chappuis minimum and looked for cluster signatures without finding them. Recent O_3-H_2O photochemical studies in cryogenic neon matrices show the quantum yield from 355 nm photolysis to be unity (15). With such visceral disagreement among laboratory studies, a thorough understanding of the effect of water on the UV–Vis absorption bands of ozone is a critical step toward providing resolution. This information is essential to elucidating the photochemistry of ozone in regions of the atmosphere of high water content and to clarifying the role of ozone–water

Significance

Ozone is one of the most important atmospheric trace gases in Earth's atmosphere. It can interact with water in the gas phase as well as with water in cloud droplet surfaces. This work identifies unique spectral signatures for ozone adsorbed at the surface of cloud water droplets in the UV and visible light domains. The adsorption process itself is thermodynamically spontaneous. With this information, it is found that the photochemistry of ozone at the air–water interface is a significant previously unidentified source of OH radicals generated at the surface of clouds. The broader implication is that the surface of cloud water droplets can be an active chemical reactor that contributes to the oxidizing capacity of the troposphere on a global scale.

Author contributions: J.M.A., M.F.R.-L., and J.S.F. designed research; J.M.A., M.M.-C., and M.F.R.-L. performed research; J.M.A., M.M.-C., M.F.R.-L., and J.S.F. analyzed data; and J.M.A., M.M.-C., M.F.R.-L., and J.S.F. wrote the paper.

The authors declare no conflict of interest.

[1]To whom correspondence may be addressed. Email: anglada@iqac.csic.es, Marilia.Martins-Costa@univ-lorraine.fr, Manuel.Ruiz@univ-lorraine.fr, or francisc@purdue.edu.

This article contains supporting information online at www.pnas.org/lookup/suppl/doi:10.1073/pnas.1411727111/-/DCSupplemental.

interactions as a potential additional source of OH radicals. The present work is an attempt to address these questions.

In Earth's atmosphere, ozone–water intermolecular interactions occur in the gas phase but they also take place in the condensed phase because ozone can be adsorbed by the surface of cloud water droplets. It is therefore important to know the spectroscopic implications of this interaction on the spectral shifts and intensities (absorption cross sections) of ozone bands. No spectroscopic studies to date have reported how water affects the spectrum of ozone at the air–water interface, despite the overall favorable energetics of the adsorption process suggested by molecular dynamics simulations based on empirical force fields (16, 17). This report provides the results of the effect of this interface on low-lying excited states of ozone from high-level ab initio calculations. First-principles molecular dynamics simulations are used to study the dynamics of ozone and determine its electronic spectrum at the air–water interface for the first time to our knowledge. The implications of the ozone spectral changes in terms of atmospheric OH production rates are evaluated and lead us to the conclusion that the photochemistry on clouds constitutes an additional source of OH radicals in the troposphere.

Results

Six singlet electronic states of ozone play a fundamental role in the photodissociation process. In Table 1, we summarize the calculations for the vertical transition energies of ozone in the gas phase obtained at the multireference configuration interaction (MRCI) level. In the UV excitation range, the Hartley band originates from photoexcitation to the 1^1B_2 and 2^1A_2 electronic states (18, 19), and the Huggins band involves the 2^1A_1 electronic state (20). These two absorption bands shield Earth's surface from the harmful UV solar emissions, protecting living organisms from harmful radiation. In the visible range, excitation to the lowest 1^1B_1 and 1^1A_2 electronic states originates from the weaker Chappuis band (18, 19). The electronic nature of this band involves transitions from the σ_{OO} ($6a_1$ and $4b_2$) and π_{OO} ($1a_2$) orbitals to the antibonding π^*_{OOO} ($2b_1$) orbital, but the absorption spectrum in this wavelength region is further complicated by multiple crossings between singlet and triplet electronic states along the potential energy surface, which opens multiple photodissociation channels (18, 19).

Crucial to the analysis of the spectral signatures of ozone at the air–water interface is the thermodynamics of the adsorption process. The free energy profile for the transfer of ozone from gas phase to bulk water is obtained from combined quantum mechanics and molecular mechanics (QM/MM) molecular dynamics simulations. Despite the hydrophobic character of ozone, for which a positive solvation free energy in water of +1.7 kcal/mol (1M → 1M) has been measured (22), our QM/MM simulations predict a significant stabilization at the air–water interface. Indeed, ozone at the interface is predicted to be more stable than ozone in gas phase (by −1.3 kcal/mol) or in bulk water (by −3.0 kcal/mol), these values being comparable to, although slightly larger than, previous estimations (16, 17). Interestingly, the average dipole moment of ozone at the air–water interface increases by almost 25% with respect to its gas-phase value, from 0.66D to 0.82D [QM/MM calculations on 1,000 snapshots from the simulations, using the Becke-3 parameter-Lee–Yang–Parr hybrid exchange-correlation functional (B3LYP) and the augmented correlation consistent-polarized valence triple zeta (aug-cc-pVTZ) basis set]. However, the modification of other electronic ground-state molecular properties is small: O–O distances and bond orders increase by *ca*. 10^{-3} Å and 10^{-3} a.u., respectively, whereas the highest occupied molecular orbital-lowest unoccupied molecular orbital gap increases by less than 2×10^{-2} eV. Data from the molecular dynamics (MD) simulations let us also make an estimation of the interface width. Fig. 1 illustrates the relative position of ozone with respect to the average interface as a function of time (data from the 100-ps MD simulation). Ozone exhibits quite large fluctuations around the interface, the position varying roughly between −4 Å, where ozone is virtually surrounded by water molecules and therefore solvation effects are comparable to bulk effects, and +4 Å, where ozone interaction with water molecules is fairly weak. The interface width can therefore be estimated to 8 Å and the molecular properties of ozone are expected to exhibit large fluctuations, between gas-phase and bulk solution values.

The calculated UV and visible light (UV–Vis) absorption spectrum of ozone at the air–water interface (convoluted MRCI/correlation consistent-polarized valence double zeta (cc-pVDZ) calculations on 300 snapshots from the QM/MM simulation) is displayed in Fig. 2 where, for comparison, we also report the spectrum of ozone in the gas phase at the same theoretical level (using in this case snapshots from a gas-phase QM MD simulation for ozone). Gas-phase experimental data (23) are also reported in Fig. 2. The agreement between the calculated and the experimental gas-phase spectrum is quite satisfying considering that, except for a systematic energy shift of the excitations (*Methods*), no scaling has been applied to the calculated oscillator strengths. Interface effects influence very slightly the position of the Hartley band maximum, although they produce an enlargement of the band in its red part (Fig. 2, *Inset A*). In addition, the calculated absorption cross section in the Chappuis band (Fig. 2, *Inset B*) shows a remarkable interface effect: The cross-section maximum increases by a factor of about 1.8, the band is red shifted by about 19 nm, and a remarkable enlargement of the band is predicted in the red side (Fig. 2, *Inset B*) [experimental estimates of solvation effects on the Chappuis

Table 1. Computed UV–Vis spectrum of ozone in gas phase

Transition	λ, nm*	f†	Characterization‡	Absorption bands
$1^1A_2 \leftarrow X^1A_1$	629.6	0.0	$4b_2 \rightarrow 2b_1$	Chappuis, ~400–790 nm
$1^1B_1 \leftarrow X^1A_1$	599.1	5.526×10^{-6}	$6a_1 \rightarrow 2b_1$	
$2^1A_1 \leftarrow X^1A_1$	294.4	1.253×10^{-6}	$4b_2^2 \rightarrow 2b_1^2 + 6a_1^2 \rightarrow 2b_1^2$	Huggins, ~310–370 nm
$1^1B_2 \leftarrow X^1A_1$	238.4	1.425×10^{-1}	$1a_2 \rightarrow 2b_1$	Hartley, < 310 nm
$2^1A_2 \leftarrow X^1A_1$	194.1	0.0	$6a_1 1a_2 \rightarrow 2b_1^2$	

Vertical transition wavelengths (λ), oscillator strengths (f), electronic characterization, and connection with absorption bands are shown. MRCI/cc-pVTZ values were computed at experimental geometry of the ground electronic state (d_{OO} = 1.273 Å, α_{OOO} = 116.75°) (21).

*The zero-point vibrational energy of the X^1A_1 state (calculated to be 0.173 eV, see *SI Text*) has not been taken into account.

†The oscillator strength is proportional to the band intensity. The $1^1A_2 \leftarrow X^1A_1$ and $2^1A_2 \leftarrow X^1A_1$ transitions are electronically dipole forbidden but vibronically allowed.

‡Relative to the ground state of O_3 (X^1A_1, which is characterized by a combination of two main electronic configurations $6a_1^2 1a_2^2 1b_1^2 4b_2^2$ and $6a_1^2 1b_1^2 2b_1^2 4b_2^2$).

CHEMISTRY

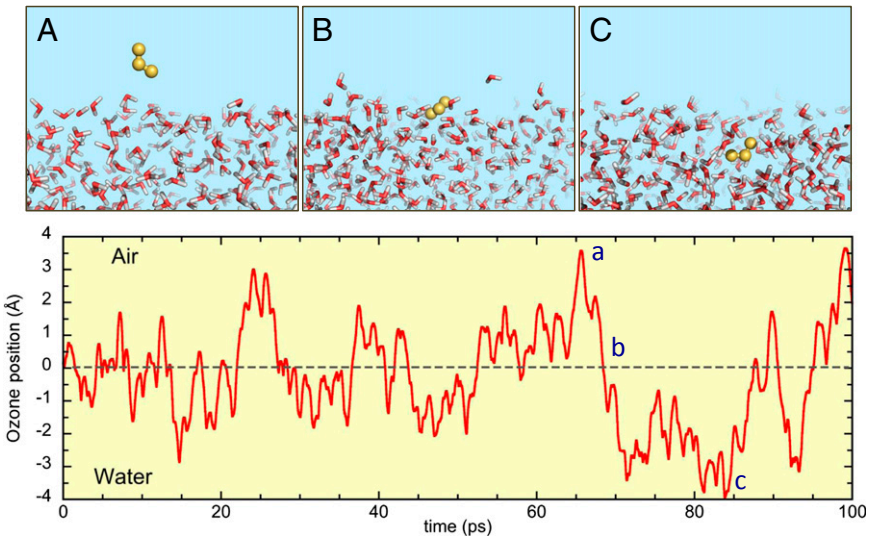

Fig. 1. Results from the 100-ps QM/MM molecular dynamics simulation. *Upper* snapshots (*A–C*) illustrate three characteristic situations of ozone (yellow) at the air–water interface with very different solvation patterns (from gas phase-like to bulk solution-like). (*Lower*) Time fluctuations of ozone center of mass with respect to the average air–water interface.

band have been reported (10, 11) in aqueous solution]. Analysis of the calculated excitation energies and oscillator strengths highlights the effect resulting from orbital interactions in the ozone–water hydrogen-bonded complexes, whereas the polarization effect due to the highly asymmetric electric field at the interface plays only a minor role. For instance, if the interface spectrum is recalculated with all water molecules being treated classically, the gas-phase Chappuis band is only slightly perturbed (the maximum of the cross section in the Chappuis band appears at 597 nm and amounts to 3.8×10^{-21} cm^2·molecule^{-1}, respectively). One might also wonder what the effect would be of treating further water molecules quantum mechanically. Such computations are too costly at the MRCI level used here but qualitative trends have been studied using time-dependent density functional theory, showing that the main effect is a significant enlargement of the Chappuis band, without an additional increase of the absorption maximum.

Discussion and Conclusions

Because ozone adsorption at the water surface produces a strong modification of the UV–Vis spectrum at wavelengths relevant to the troposphere, the photolysis rate and the subsequent chemistry may be significantly changed. The photolysis rate constant is defined as

$$J = \sum_{\lambda} \sigma(\lambda)\phi(\lambda)q(\lambda),$$

where σ is the ozone absorption cross section, ϕ is the quantum yield, q is the actinic flux, and λ is the wavelength. Both, σ and ϕ depend on the molecular environment of ozone—gas phase or interface. Moreover, it is well known that multiple dissociation pathways are possible for ozone. The spin-allowed photolysis of ozone in the Hartley absorption band is the dominant process,

$$O_3 + h\nu(\lambda < 310 \text{ nm}) \rightarrow O(^1D) + O_2(a^1\Delta_g), \qquad [4]$$

although in the lower atmosphere, photolysis through this channel is limited to wavelengths higher than 290 nm because the actinic flux decays to zero at shorter wavelengths. Laboratory experiments (24) have shown, however, that there is a significant tail for the O(^{1}D) quantum yield beyond 310 nm and it has been argued that this is due to the contribution of the spin-forbidden channel [with energetic threshold ~411 nm (24)]:

$$O_3 + h\nu(\lambda < 411 \text{ nm}) \rightarrow O(^1D) + O_2\left(X^3\Sigma_g^-\right). \qquad [5]$$

Recommended O(^{1}D) quantum yields in the 290- to 350-nm range can be found in the work reported by Matsumi et al. (24).

Another spin-allowed process that is in principle attainable even at higher wavelengths leads to the formation of atomic and molecular oxygen in their ground electronic states

$$O_3 + h\nu(\lambda < 1180 \text{ nm}) \rightarrow O(^3P) + O_2\left(X^3\Sigma_g^-\right), \qquad [6]$$

for which the quantum yield in the Chappuis band is unity (25). In the troposphere, this reaction is considered to play a negligible role in the gas-phase chemistry of ozone owing to a fast recombination rate. However, for ozone at a water interface, this photolytic pathway becomes relevant because the reaction of O(^{3}P) with water to form two OH radicals is energetically accessible in the Chappuis band region. This reaction has been investigated in the literature (26, 27) but to get very accurate energy values, we have revisited the process by performing geometry optimizations at the quadratic configuration interaction level with single and double excitations (QCISD) using the aug-cc-pVTZ basis set, and carrying out single-point energy calculations at the coupled cluster level with a full treatment of single and double excitations and a perturbative correction for triple excitations [CCSD(T)] extrapolated to the complete basis set (CBS) limit. Table 2 shows that our calculations predict this reaction to be endothermic by 15.92 kcal·mol^{-1}, which is in excellent agreement with the experimental value of 15.85 kcal·mol^{-1} (28). Our calculations also show that for the reaction to occur, an energy barrier of 17.65 kcal·mol^{-1} needs to be surmounted. Taking into account that ozone is photoexcited from its first vibrational level of the ground state and that the experimental dissociation energy for the process O_3 (X^1A_1) → O(^3P_g) + O_2 ($^3\Sigma_g^-$) is 24.26 kcal·mol^{-1} (28), one can deduce that for the reaction to occur after ozone photolysis, an energy excess of 41.91 kcal·mol^{-1} is needed, which corresponds to an excitation energy of 1.82 eV, roughly 700 nm.

In the gas phase, the primary fate of O(^{1}D) is collisional deactivation to the triplet ground state (quenched by species such

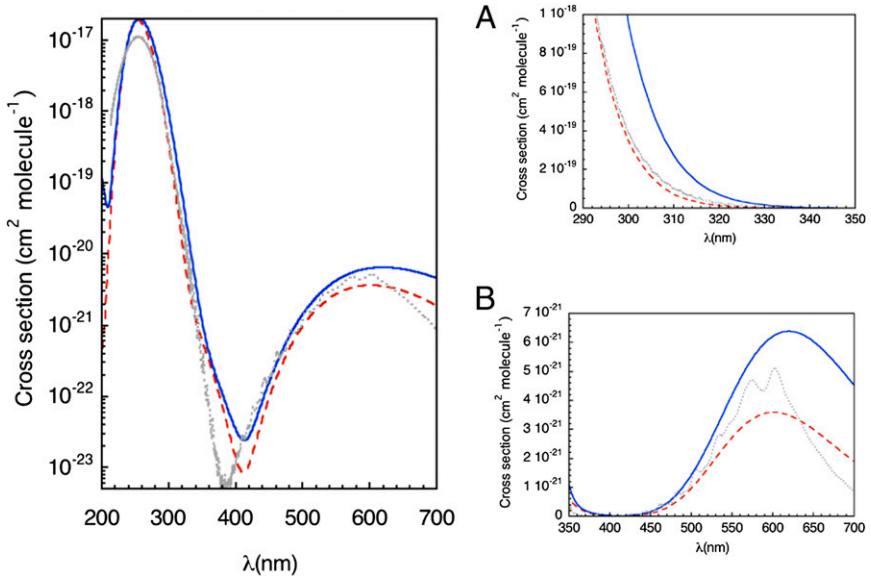

Fig. 2. Calculated UV–Vis spectrum of ozone in gas phase (red, dashed line) and at the air–water interface (blue, solid line), compared with the gas-phase experimental spectrum (23) (gray, dotted line) (logarithmic scale). (*Right*) *Insets A* and *B* (linear scale) show some details of the spectra in the UV and visible regions, respectively, relevant for photochemistry in the troposphere. Maxima of the calculated cross sections appear at 254 nm ($\sigma = 1.9 \times 10^{-17}$) and 601 nm ($\sigma = 3.6 \times 10^{-21}$) in gas phase and at 256 nm ($\sigma = 2.0 \times 10^{-17}$) and 620 nm ($\sigma = 6.4 \times 10^{-21}$) at the air–water interface; experimental data in gas phase show maxima at 253.7 nm ($\sigma = 1.1 \times 10^{-17}$) and 602 nm ($\sigma = 5.1 \times 10^{-21}$) ($\sigma$ values are in cm^2·molecule^{-1}).

as N_2, O_2, or CO_2) and only a small fraction of $O(^1D)$ reacts with water or methane to form OH radicals, according to reactions 2 and 3. The overall OH production rate associated to ozone photolysis can therefore be written as

$$\frac{d[OH]}{dt} = -f_{OH}\frac{d[O_3]}{dt} = f_{OH}J_{O_3}[O_3],$$

where f_{OH} represents the fraction of $O(^1D)$ atoms leading to OH formation. Typical values of f_{OH} in the marine boundary layer amount to about 10% (29) but an average value in the troposphere is more likely 3% (30). Using previously reported actinic flux values (31) (at Earth's surface, noontime, and no surface Albedo) and $O(^1D)$ quantum yields (24), we have estimated a photolysis rate constant $J_{O_3} = 3.2 \times 10^{-5}$ s^{-1}, which is in excellent agreement with the value 3.8×10^{-5} s^{-1} (9) estimated from experimental data in similar conditions (12), as well as with available experimental values in slightly different conditions (values in the range $0.42–6 \times 10^{-5}$ s^{-1}) (25, 32, 33). Likewise, using a typical ozone concentration of 7.5×10^{11} molecules·cm^{-3} for the gas-phase ozone concentration at Earth's surface (9, 25) and $f_{OH} = 3\%$, we deduce an OH production rate of 0.7×10^6 molecules·cm^{-3}·s^{-1} for the bimolecular reaction of $O(^1D)$ with water, which again is in nice agreement with measured daytime rates falling in the range $0.7–10 \times 10^6$ molecules·cm^{-3}·s^{-1} (34, 35).

Table 2. Zero-point energies (ZPE), relative energies (ΔE), and relative energies with ZPE (Δ(E + ZPE)) computed for the $O(^3P_g) + H_2O \rightarrow 2OH$ reaction

Compound	ZPE	ΔE	Δ(E + ZPE)
$O(^3P_g) + H_2O$	13.4 (0.58)	0.00 (0.00)	0.00 (0.00)
TS	10.0 (0.43)	21.12 (0.92)	17.65 (0.77)
2OH	10.7 (0.46)	18.62 (0.81)	15.92 (0.69)*

Values are in kcal·mol^{-1} and eV (in parentheses). ZPE values are computed at the QCISD/aug-cc-pVTZ level of theory. The energies are computed at the CCSD(T)/CBS level of theory on QCISD/aug-cc-pVTZ optimized geometries.
*The experimental value is 15.85 kcal·mol^{-1} (0.69 eV).

The excellent results obtained in the gas phase for the photolysis rate constant and OH production rate validate our computational methodology and more specifically the calibration of the UV–Vis absorption energies. We now use the same methodology and the results of first-principles molecular dynamics simulations to estimate the OH production rate at the air–water interface. To this aim, we assume that all oxygen atoms produced in the ozone photolysis at the interface do immediately react with the surrounding water molecules. The following rate equation can then be used (where $[O_3]_{int}$ represents the ozone concentration at the air–water interface, and $J^{int}_{O_3}$ is the associated photolysis rate constant):

$$\frac{d[OH]}{dt} = -2\frac{d[O_3]_{int}}{dt} = 2J^{int}_{O_3}[O_3]_{int}.$$

For the O_3 on-water concentration, we take the value $[O_3]_{int} = 9.6 \times 10^{12}$ molecules·cm^{-3}, which has been estimated from the gas-phase ozone concentration used above and the solvation free energies obtained from our work (our estimated concentration of ozone in bulk water in these conditions is 4.2×10^{10} molecules·cm^{-3}). The photolysis rate constant at the interface is unknown. An upper limit can be estimated by assuming that the photolytic channels leading to either $O(^1D)$ or $O(^3P)$ are all active, because as mentioned above, they are energetically accessible (quantum yield unity). A lower limit can be obtained by assuming that only $O(^1D)$ channels are active. The calculations lead, respectively, to $J^{int}_{O_3} = 7.6 \times 10^{-4}$ s^{-1} and $J^{int}_{O_3} = 1.1 \times 10^{-4}$ s^{-1}. From these values, we calculate an OH production rate at the air–water interface in the range $0.21–1.5 \times 10^{10}$ molecules·cm^{-3}·s^{-1}, to be compared with our calculated production rate in the gas phase, 0.7×10^6 molecules·cm^{-3}·s^{-1}. The upper limit for the OH production rate at the air–water interface is therefore predicted to be about three to four orders of magnitude larger than in the gas phase. In this estimation, the visible light contribution (450–700 nm) is found to be larger than the UV one (290–450 nm) by approximately a factor of 2. The OH radicals produced in this way may undergo desorption from the air–water interface and hence enter into the gas phase. However, OH radicals exhibit a marked affinity for the air–water interface (16, 17), with a relative interface/gas concentration estimated to be *ca.* $10^3–10^4$,

Table 3. Ozone photolysis rate constants (J) and OH production rates (v_{OH}) in the gas phase and at the air–water interface

	Gas phase		Air–water interface	
	J, s^{-1}	v_{OH}, molecule·cm^{-3}·s^{-1}	J, s^{-1}	v_{OH}, molecule·cm^{-3}·s^{-1}
Calculated, this work	3.2×10^{-5}	0.7×10^{6}	7.6×10^{-4}*	1.5×10^{10}
			1.1×10^{-4}†	0.21×10^{10}
Measured‡	3.8×10^{-5}	$0.7–10 \times 10^{6}$	—	—

Calculations assume a gas-phase concentration of ozone equal to 7.5×10^{11} molecules·cm^{-3}, $T = 298$ K, and actinic flux at Earth's surface, noontime, with surface's Albedo of zero.

*Calculations assuming that all photolytic channels [O(^{1}D) and O(^{3}P)] are active (quantum yield unity).

†Calculations assuming that only O(^{1}D) channels are active (quantum yields from ref. 24).

‡The photolysis rate constant is taken from ref. 9 and the OH production rate is taken from refs. 34 and 35.

and therefore our results suggest that ozone photolysis at the surface of cloud water droplets can significantly contribute to the production of OH radicals at the interface of cloud surfaces.

The calculated ozone photolysis rate constant and OH formation rates are summarized in Table 3. The actual OH production depends of course on the water surface per volume unit ratio, which is usually quite large in clouds. For instance, for an average droplet radius of 10^{-6} m and a volume fraction of liquid water in clouds of 10^{-6} (36) the water surface/volume ratio is about 3 cm^2·L^{-1}. The relatively high water surface/volume ratio in clouds is thought to be responsible for significant heterogeneous chemistry in the troposphere, as shown in recent airborne measurements of methanol gas-phase concentration when a smoke plume intersected a cumulus cloud (37). Our data suggest that heterogeneous reactions might explain the observed rapid loss of methanol and simultaneous production of formaldehyde. Our results further suggest that ozone photolysis at the surface of water droplets can significantly contribute to the production of OH radicals at the interface. The additional radicals produced in this way may undergo desorption from the droplets, entering into the gas phase, where they can participate in atmospheric oxidation processes. However, they are also likely to react in situ, in accord with suggestions from other simpler models (38). Hydroxyl radicals can either recombine to form hydrogen peroxide (therefore modulating the OH activity deduced from our upper-limit OH production rate) or participate in oxidation reactions with adsorbed organic compounds. In summary, the surface of cloud water droplets can be an active chemical reactor that contributes to the oxidizing capacity of the troposphere on a global scale. The findings of this study suggest that gas-phase OH radical chemistry may not be the only initiator of oxidation of organics in the troposphere, but cloud surfaces could be a new additional source, in agreement with well-known examples of interface chemistry involving inorganic and organic species in the lower atmosphere (39).

This work has several important broader implications. It shows an important role of aerosols and clouds beyond their function as a reflective/scattering radiation source in the overall atmospheric radiation balance. In particular, it shows that the air–water interface could stimulate photochemistry on aerosol/clouds surfaces. Interface effects appear to be significant and are found to have a strong influence on the ozone Chappuis band, specifically showing an enhancement of the cross-section maximum, which is increased by a factor of about 1.8, as well as a red shift and enlargement on the red side of the band. Matthews et al. (40) showed the importance of weak electronic absorption features in contributing to OH radical production in the gas-phase photochemistry in the troposphere, as a result of photochemistry in the electronic absorption tail. Our results show that the spectral perturbations exerted on ozone by the interface, which show the generation of electronic absorption tails in the relevant ozone bands, should lead to a marked enhancement of OH radical production at the interface. As far as UV penetrates optically thin clouds but not thick clouds, the conclusions above should principally apply for photochemistry in thin cirrus clouds (which are ubiquitous, even in "clear" skies) and at the top of dense clouds. They should also be taken into consideration for the explanation of OH enhancement in high aerosol concentrations, as the latter tend to have liquid water coatings.

Methods

The absorption spectrum of ozone at the air–water interface is obtained through a combination of first-principles MD simulations and MRCI calculations. MD simulations are carried out for the ozone molecule interacting with a slab of water molecules, using a combined QM/MM approach. Ozone is described quantum mechanically [B3LYP/6–311+G(d) level], with water molecules being described classically (using the three-point transferable intermolecular potential, TIP3P). Such a scheme allows for electrostatic embedding; i.e., the net atomic charges on water molecules polarize the electronic distribution of ozone. The effect of potential ions dissolved in the droplet has not been taken into account, so that our model corresponds to an aqueous medium with low ionic strength. The simulation box contains ozone and 499 water molecules and we apply periodic boundary conditions along the X and Y directions. After equilibration (canonical ensemble, $T = 298$ K), the simulation is carried out for 100 ps. To calculate the time-averaged UV–Vis absorption spectrum, the following computational protocol is used. From the simulation, a set of 300 snapshots is selected. For each snapshot, the water molecules within a cutoff radius of 12 Å around ozone are explicitly considered. Ozone and the closest water molecule are treated quantum mechanically in the electronic spectrum calculations whereas the remaining water molecules are treated classically; they generate an electrostatic embedding of the ozone–water complex. The spectra are calculated at the MRCI/cc-pVDZ level. The average spectrum is obtained by a convolution of the 300 MRCI calculations. To account for both vibrational quantum effects (zero-point energy) and errors connected with different approximations in the methodology, we have applied a systematic energy correction to the calculated absorption energies, as described in *SI Text*, which provides also further details on the computational approach.

ACKNOWLEDGMENTS. The authors are grateful to the Centre de Supercomputació de Catalunya, the Spanish Centro Técnico de Informática–Consejo Superior de Investigaciones Cientificas, and the French Centre Informatique National de l'Enseignement Supérieur (project LCT2550) for providing computational resources. This work was supported by the Spanish Dirección General de Investigación Científica y Técnica (CTQ2011-27812), the Generalitat de Catalunya (Grant 2014SGR139), the Centre National de la Recherche Scientifique and the University of Lorraine in France, and the National Science Foundation.

1. Haigh JD, Winning AR, Toumi R, Harder JW (2010) An influence of solar spectral variations on radiative forcing of climate. *Nature* 467(7316):696–699.
2. Shindell DT, et al. (2009) Improved attribution of climate forcing to emissions. *Science* 326(5953):716–718.
3. Levy H, 2nd (1971) Normal atmosphere: Large radical and formaldehyde concentrations predicted. *Science* 173(3992):141–143.
4. Kley D, et al. (1996) Observations of near-zero ozone concentrations over the convective Pacific: Effects on air chemistry. *Science* 274(5285):230–233.

5. Di Carlo P, et al. (2004) Missing OH reactivity in a forest: Evidence for unknown reactive biogenic VOCs. *Science* 304(5671):722–725.
6. Hofzumahaus A, et al. (2009) Amplified trace gas removal in the troposphere. *Science* 324(5935):1702–1704.
7. Wennberg PO, et al. (1999) Twilight observations suggest unknown sources of HO_x. *Geophys Res Lett* 26(10):1373–1376.
8. Wennberg PO, Dabdub D (2008) Atmospheric chemistry. Rethinking ozone production. *Science* 319(5870):1624–1625.
9. Frost G, Vaida V (1995) Atmospheric implications of the photolysis of the ozone-water weakly-bound complex. *J Geophys Res* 100(D9):18803–18809.
10. Vaida V, Donaldson DJ, Strickler SJ, Stephens SL, Birks JW (1989) A reinvestigation of the electronic spectra of ozone - condensed phase effects. *J Phys Chem* 93(2):506–508.
11. Vaida V (2011) Perspective: Water cluster mediated atmospheric chemistry. *J Chem Phys* 135(2):020901.
12. Hurwitz Y, Naaman R (1995) Production of OH by dissociating ozone–water complexes at 266 and 355 nm and by reacting $O(^1D)$ with water dimers. *J Chem Phys* 102(5):1941–1943.
13. Jin B, Su M-N, Lin JJ-M (2012) Does ozone-water complex produce additional OH radicals in the atmosphere? *J Phys Chem A* 116(49):12082–12088.
14. Axson JL, et al. (2011) Absolute ozone absorption cross section in the Huggins Chappuis minimum (350-470 nm) at 296 K. *Atmos Chem Phys* 11(22):11581–11590.
15. Tsuge M, Tsuji K, Kawai A, Shibuya K (2013) Photochemistry of the ozone-water complex in cryogenic neon, argon, and krypton matrixes. *J Phys Chem A* 117(49): 13105–13111.
16. Vacha R, Slavicek P, Mucha M, Finlayson-Pitts BJ, Jungwirth P (2004) Adsorption of atmospherically relevant gases at the air/water interface: Free energy profiles of aqueous solvation of N_2, O_2, O_3, OH, H_2O, HO_2, and H_2O_2. *J Phys Chem A* 108(52): 11573–11579.
17. Vieceli J, et al. (2005) Molecular dynamics simulations of atmospheric oxidants at the air-water interface: Solvation and accommodation of OH and O3. *J Phys Chem B* 109(33):15876–15892.
18. Banichevich A, Peyerimhoff SD, Grein F (1993) Potential energy surfaces of ozone in its ground state and in the lowest-lying eight excited states. *Chem Phys* 178(1-3): 155–188.
19. Grebenshchikov SY, Qu ZW, Zhu H, Schinke R (2007) New theoretical investigations of the photodissociation of ozone in the Hartley, Huggins, Chappuis, and Wulf bands. *Phys Chem Chem Phys* 9(17):2044–2064.
20. O'Keeffe P, Ridley T, Lawley KP, Donovan RJ (2001) Re-analysis of the ultraviolet absorption spectrum of ozone. *J Chem Phys* 115(20):9311–9319.
21. Tyuterev VG, Tashkun S, Jensen P, Barbe A, Cours T (1999) Determination of the effective ground state potential energy function of ozone from high-resolution infrared spectra. *J Mol Spectrosc* 198(1):57–76.
22. Sander R (1999) *Compilation of Henry's Law Constants for Inorganic and Organic Species of Potential Importance in Environmental Chemistry*, Version 3. Available at http://www.henrys-law.orgreference.
23. Gorshelev V, Serdyuchenko A, Weber M, Chehade W, Burrows JP (2013) High spectral resolution ozone absorption cross-sections – Part 1: Measurements, data analysis and comparison with previous measurements around 293K. *Atmos Meas Tech Discuss* 6:6567–6611.
24. Matsumi Y, et al. (2002) Quantum yields for production of O(1D) in the ultraviolet photolysis of ozone: Recommendation based on evaluation of laboratory data. *J Geophys Res* 107(D3):ACH 1-1–ACH 1-12.
25. Warnek P, Williams J (2012) *The Atmospheric Chemist's Companion: Numerical Data for Use in the Atmospheric Science* (Springer, Dordrecht, The Netherlands).
26. Brunsvold AL, et al. (2007) Crossed-beams and theoretical studies of the O((3)P) + H(2) O —> HO(2) + H reaction excitation function. *J Phys Chem A* 111(43):10907–10913.
27. Conforti PF, Braunstein M, Braams BJ, Bowman JM (2010) Global potential energy surfaces for $O(^{(3)}P) + H_2O(^{(1)}A_1)$ collisions. *J Chem Phys* 133(16):164312.
28. Argonne National Laboratory (2014) *Active Thermochemical Tables*. Available at http://atct.anl.gov/Thermochemical%20Data/version%201.110/index.html. Accessed March 26, 2014.
29. Monks PS (2005) Gas-phase radical chemistry in the troposphere. *Chem Soc Rev* 34(5): 376–395.
30. Lelieveld J, Peters W, Dentener FJ, Krol MC (2002) Stability of tropospheric hydroxyl chemistry. *J Geophys Res* 107(D23):4715.
31. Finlayson-Pitts BJ, Pitts JN, Jr (1986) *Atmospheric Chemistry: Fundamental and Experimental Techniques* (Wiley, New York).
32. Kelley P, Dickerson RR, Luke WT, Kok GL (1995) Rate of NO_2 photolysis from the surface to 7.6 km altitude in clear-sky and clouds. *Geophys Res Lett* 22(19):2621–2624.
33. Seinfeld JH, Pandis SN (2006) *Atmospheric Chemistry and Physics: From Air Pollution to Climate Change* (Wiley, New York), 2nd Ed.
34. Perner D, et al. (1987) Measurements of tropospheric OH concentrations: A comparison of field data with model predictions. *J Atmos Chem* 5(2):185–216.
35. Stone D, Whalley LK, Heard DE (2012) Tropospheric OH and HO_2 radicals: Field measurements and model comparisons. *Chem Soc Rev* 41(19):6348–6404.
36. Lelieveld J, Crutzen PJ (1991) The role of clouds in tropospheric photochemistry. *J Atmos Chem* 12:229–267.
37. Tabazadeh A, et al. (2004) Heterogeneous chemistry involving methanol in tropospheric clouds. *Geophys Res Lett* 31(6):L06114.
38. Du S, Francisco JS (2008) Interaction between OH radical and the water interface. *J Phys Chem A* 112(21):4826–4835.
39. Finlayson-Pitts BJ (2009) Reactions at surfaces in the atmosphere: Integration of experiments and theory as necessary (but not necessarily sufficient) for predicting the physical chemistry of aerosols. *Phys Chem Chem Phys* 11(36):7760–7779.
40. Matthews J, Sinha A, Francisco JS (2005) The importance of weak absorption features in promoting tropospheric radical production. *Proc Natl Acad Sci USA* 102(21): 7449–7452.